RSC Advances

PAPER

View Article Online
View Journal | View Issue

Cite this: *RSC Adv.*, 2021, **11**, 37624

Rapid large-scale synthesis of ultrathin NiFe-layered double hydroxide nanosheets with tunable structures as robust oxygen evolution electrocatalysts†

Changmin Hou, Zhao Cui, Sai Zhang, Wenlong Yang,* Hongtao Gao and Xiliang Luo*

Transition metal layered double hydroxides (LDHs) with ultrathin two-dimensional (2D) structures, especially NiFe-based LDH nanosheets, have been extensively developed as advanced oxygen evolution reaction (OER) electrocatalysts for water splitting. Nevertheless, traditional synthetic approaches for these promising catalysts usually involve tedious pretreatment procedures and a subsequent time-consuming exfoliation process, and the obtained products possess a wide dispersion of thickness and limited production yield. Here, a sequence of ultrathin NiFe-LDH nanosheets with tunable components were prepared on a large scale *via* a rapid room-temperature method under ambient conditions, and were further used as a desired material model for studying the influence of Ni/Fe ratio modulation on the OER performance. Due to the synergetic effect of more exposed active sites, efficient electron transport and optimized OER kinetics, the resulting LDH samples manifest outstanding electrocatalytic performance toward water oxidation.

Received 30th June 2021
Accepted 13th November 2021

DOI: 10.1039/d1ra05045a

rsc.li/rsc-advances

Introduction

Electrocatalytic water splitting has received considerable research interest owing to its renewable and high-efficiency hydrogen production for mitigating the growing energy demands and worsening environment issues.[1–5] However, the electrochemical energy conversion efficiency has been largely restricted by the oxygen evolution reaction (OER) because of its sluggish anode kinetics.[6–8] To date, although noble-metal-based materials including RuO_2 and IrO_2 have emerged as the most efficient catalysts to drive the complex OER process, the high cost and extreme scarcity largely limit their extensive usage in the field of energy conversion.[9,10] Until now, continuous efforts have been made to develop cost-effective 3d transition metals and derivatives as promising alternatives to noble metals. Among these catalysts, layered double hydroxides (LDHs) based on transition metals (Fe, Co, Ni) have drawn plenty of attention due to their easy availability, novel electrical property and high catalytic activity.[11–18] Of note, their intrinsic layered structure renders the production of ultrathin two dimensional (2D) nanosheets feasible, which could endow them with highly exposed active sites and modified electronic structures for optimizing the electrocatalytic OER performance.[19,20] In general, there are two main strategies for synthesizing ultrathin LDHs nanosheets: top-down and bottom-up approaches.[21,22] Even though the top-down synthesis is the most widely used approach, its synthetic procedures usually involve complicated ion-exchange treatment or prolonged exfoliation times in appropriate solvents, and the as-exfoliated LDHs nanosheets show a wide size or thickness distribution, these shortcomings unfortunately block the practical application of this synthetic strategy. By contrast, the bottom-up synthesis requires fewer synthetic procedures, is considered comparatively simple and convenient. However, organic solvents or surfactants applied in the synthetic process are usually absorbed on the nanosheets surface and hard to be removed, which would inevitably impede the contact between active sites and the electrolyte, thus suppressing the overall electrochemical performance. Of particular note is that, the production yield of LDHs nanosheets obtained by above-mentioned methods is still relatively low and needs to be further boosted for large-scale applications. Therefore, it is highly imperative but challenging to develop a simple and time-saving method for synthesizing high-efficiency ultrathin LDHs nanosheets electrocatalysts on a large scale to meet the requirement of commercial development. On the other hand, from a componential manipulation point of view, the modulation of metal ratios in LDHs nanosheets could exert a significant

Key Laboratory of Optic-electric Sensing and Analytical Chemistry for Life Science, MOE, Key Laboratory of Analytical Chemistry for Life Science in Universities of Shandong, College of Chemistry and Molecular Engineering, Qingdao University of Science and Technology, Qingdao 266042, P. R. China. E-mail: wlyang@qust.edu.cn; xiliangluo@qust.edu.cn

† Electronic supplementary information (ESI) available. See DOI: 10.1039/d1ra05045a

influence on their electronic structures and physicochemical properties, thus offering the opportunity to optimize the overall electrochemical performance of LDHs catalysts. Unfortunately, due to the lack of ideal catalytic model for investigating the underlying effect of metal atom ratios on the OER activity, the fundamental understanding of the related mechanism for efficient water oxidation is still under debate.

Bearing these considerations in mind, herein, we present an effective room-temperature co-precipitation route to achieve a series of ultrathin and tunable composition of NiFe-LDH samples, as well as the utilization of these obtained LDHs nanosheets as highly efficient electrocatalysts toward water oxidation. Most interestingly, the formation of precipitation in a liquid-phase reaction was quickly accomplished by the addition of ammonium hydroxide into an aqueous solution containing ammonium persulfate, Ni^{2+} and Fe^{3+} ions under ambient atmospheric conditions (see details in the ESI†), which can be availably scaled up to gram-level yield just by increasing the size of vessel at low cost. Moreover, taking NiFe-LDHs nanosheets with different metal ratios as the proof-of-concept prototype, we highlight the crucial role of metal atom ratios during the electrocatalytic OER process in virtue of a combination of theoretical calculations and experimental investigations. In terms of electrochemical results, the obtained LDHs samples show robust electrocatalytic activity for OER. In particular, ultrathin Ni_2Fe_1-LDHs nanosheets exhibit a small overpotential of 263 mV ($j = 10$ mA cm^{-2}) and a quite high current density of 349.1 mA cm^{-2} at a potential of 1.8 V *vs.* RHE, which are demonstrated as high-efficiency non-precious-metal electrocatalysts toward water oxidation.

Experimental

Materials

All reagents in this study were of analytical reagent grade, which were purchased from Sinopharm Chemical Reagent Co., Ltd., and utilized as received without any purification.

Synthesis of ultrathin NiFe-LDHs nanosheets

In a typical procedure, a certain amount of $NiCl_2 \cdot 6H_2O$ and $FeCl_3 \cdot 6H_2O$ (with total quantity of 1 mmol) and ammonium persulfate aqueous solution (0.5 mmol) were dissolved in 200 mL water at room temperature under vigorous magnetic stirring for 5 minutes. Then, 1 mL of 28% ammonia solution was added into the above solution drop by drop with vigorous magnetic stirring. After a few minutes of sedimentation, the resulting precipitation was isolated by centrifugation and washed with distilled water and ethanol several times, then dried at 60 °C in air overnight for further characterization. The other NiFe-LDHs samples with different Ni/Fe atomic ratio were synthesized by changing the ratio of starting materials.

Synthesis of ultrathin NiCo-, CoFe-based nanosheets

The synthetic procedure for NiCo-, CoFe-based ultrathin nanosheets was similar to that for the ultrathin NiFe-LDHs nanosheets, except that tuning the collocation of starting materials of $NiCl_2 \cdot 6H_2O$, $CoCl_2 \cdot 6H_2O$ and $FeCl_3 \cdot 6H_2O$ while keeping their total dose at 1 mmol.

Characterization

Powder X-ray diffraction patterns (XRD) were measured on Japan Rigaku D/max-rA equipped with graphite monochromatized high-intensity Cu Kα radiation ($\lambda = 1.54178$ Å). The transmission electron microscopy (TEM) images were performed on a H-7650 (Hitachi, Japan) operated at an acceleration voltage of 100 kV. X-ray photoelectron spectroscopy (XPS) valence spectra were conducted on an ESCALAB MKII X-ray photoelectron spectrometer with an excitation source of Mg Kα = 1253.6 eV. The Fourier transform infrared (FT-IR) spectra were recorded on a NICOLET FT-IR spectrometer in KBr tablets, scanning from 4000 to 400 cm^{-1} at room temperature.

Electrochemical measurements

All electrochemical tests were performed in 1 M KOH solution on an electrochemical station (CHI660B) by using Ag/AgCl (3.3 M KCl) electrode as the reference electrode, a graphite electrode as the counter electrode, and a glassy carbon (GC, 3 mm in diameter) electrode with different catalysts as the working electrode. Typically, 4 mg of catalysts and 30 μL of 5 wt% Nafion solutions (Sigma-Aldrich) were dispersed in 1 mL of water–isopropanol solution with volume ratio of 3 : 1 by sonicating for 1 h to form a homogeneous ink. Then, 5 μL of the obtained dispersion (about 20 μg of catalyst) was loaded onto a GC electrode (loading 0.285 mg cm^{-2}). Linear sweep voltammetry curves was carried out at a scan rate of 5 mV s^{-1}. Electrochemical impedance spectroscopy (EIS) measurements were recorded at 0.45 V *vs.* Ag/AgCl. The amplitude of the applied voltage was 5 mV, and the frequency range was 100 kHz to 1 Hz.

Calculation method

All calculations were performed within density functional theory (DFT) framework in the Vienna *ab initio* simulation package (VASP) software packages.[39,40] The exchange–correlation energy of electrons was described within the generalized gradient approximation (GGA) framework using the Perdew–Burke–Ernzerhof (PBE) functional.[41] The strong-correlated correction in NiO is considered by GGA + U method with a U–J value of 6 eV for Ni atom.[42] The model of NiFe-LDHs was simulated by Fe replacing Ni atom in a 5 × 6 × 1 supercell containing 30 Ni atoms. The plane-wave cutoff energy of 350 eV and 5 × 5 × 1 (1 × 1 × 1) k-points were used for electronic calculations within the Monkhorst–Pack scheme. In view of the characteristics of layered accumulation in model, van der Waals correction is incorporated to further describe the weak interlayer interaction.[43] All geometric structures were fully relaxed and optimized until the force on the atoms was less than 0.05 eV Å^{-1}, and the convergence criterion for the electron self-consistency was set to 1.0 × 10^{-4} eV.

Results and discussion

In this study, a series of high-quality ultrathin Ni_xFe_y-LDH nanosheets with different components (Ni/Fe atomic ratio = x/

y) were synthesized by means of aforesaid liquid-phase synthesis process, during which the Ni/Fe atomic ratio in LDH nanosheets was easily adjusted by tuning the Ni/Fe ratio of the starting materials. Transmission electron microscopy (TEM) analysis was firstly performed to survey the morphology of as-obtained samples. As can be seen from the TEM images in Fig. 1, all NiFe-LDHs samples are of typical platelet-like morphology and their almost transparent feature to the electron beams reflects the ultrathin nature of NiFe-LDHs nanosheets. Of note, the high-resolution TEM image of Ni_2Fe_1-LDHs sample shows legible lattice fringes with interplanar distance of 0.257 and 0.198 nm in Fig. S1,† corresponding to the (012) and (018) planes of NiFe-LDHs, respectively. Furthermore, X-ray diffraction (XRD) was applied to detect the structural information of collected powdery LDHs products. As shown in Fig. 2A, all XRD patterns can be well indexed to the characteristic LDH structure of NiFe compounds (JCPDS no. 40-0215), confirming the successful preparation of NiFe-LDHs. Fourier transform infrared spectroscopy (FTIR) in Fig. S2† further certifies the formation of NiFe-LDHs. Moreover, X-ray photoelectron spectroscopy (XPS) was used to characterize the surface compositions and chemical states of Ni_xFe_y-LDHs samples. The XPS survey spectrum (Fig. S3†) clearly demonstrates that all NiFe-LDHs samples consist of the Fe, Ni and O elements and no other impurities can be identified, suggesting the formation of pure NiFe-LDHs, consistent with the XRD analysis. In the high-resolution Ni 2p spectrum of Ni_2Fe_1-LDHs sample (Fig. 2B), except for two shakeup satellites (denoted as "Sat.") centered at 861.6 and 879.6 eV, the spin–orbit doublets positioned at 855.7 and 873.5 eV with the spin-energy separation of 17.8 eV can be respectively ascribed to Ni $2p_{3/2}$ and Ni $2p_{1/2}$, which is indicative of the presence of Ni^{2+} ions. As shown in Fig. 2C, the Fe 2p spectrum of Ni_2Fe_1-LDHs was deconvoluted into four distinct

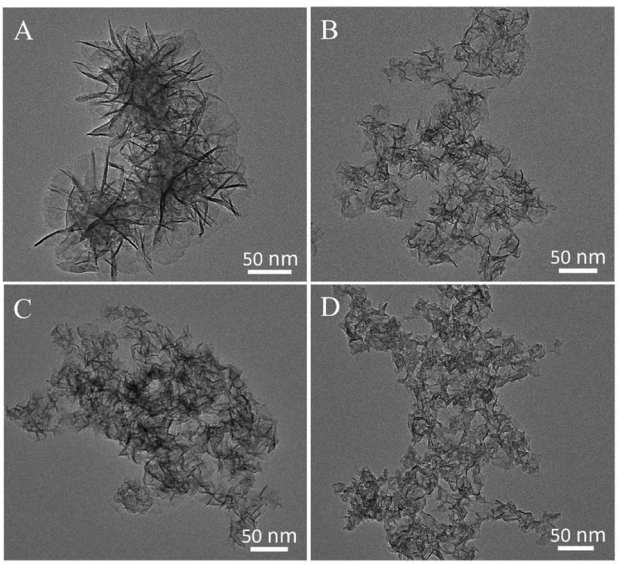

Fig. 1 TEM images of various NiFe-LDHs samples prepared at room temperature by the co-precipitation method: (A) Ni_9Fe_1-LDHs, (B) Ni_4Fe_1-LDHs, (C) Ni_2Fe_1-LDHs and (D) Ni_1Fe_1-LDHs.

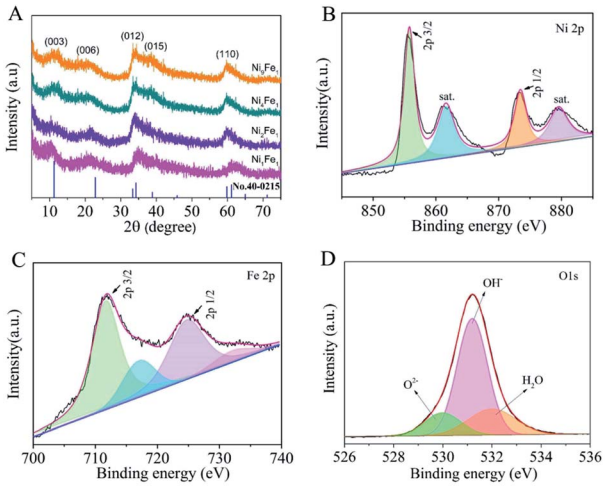

Fig. 2 (A) XRD patterns for various NiFe-LDHs samples. XPS spectra of (B) Ni 2p, (C) Fe 2p and (D) O 1s for Ni_2Fe_1-LDHs sample.

peaks positioned at 711.7, 717.3 eV, 724.9 and 732.3 eV, which can be fairly assigned to Fe $2p_{3/2}$, Fe $2p_{1/2}$, respectively, and their corresponding satellite peaks, verifying the presence of Fe^{3+} in the NiFe-LDHs sample. While the O 1s spectrum in Fig. 2D can be fitted into three legible peaks located at around 530.0, 531.2 and 532.0 eV, which agree well with the binding energies of O^{2-}, OH^- and adsorbed water, respectively. Especially, in comparison with the other two peaks, the prominent OH^- peak confirms that hydroxide is the main existing form of O atoms in Ni_2Fe_1-LDHs sample.[23–26] Next, inductively coupled plasma atomic emission spectrometry results in Table S1† reveal that the Ni/Fe atomic ratios for Ni_9Fe_1, Ni_4Fe_1, Ni_2Fe_1, Ni_1Fe_1 samples are about 8.81, 4.14, 2.03, 1.05, respectively, which are fairly coincided with the ratio values of their starting materials, implying the adjustable chemical compositions of NiFe-LDHs samples. Of note, TEM images in Fig. S4† confirm that this simple co-precipitation method can be employed as an effective strategy for synthesizing other transition-metal nanosheets with ultrathin thickness and tunable components, reflecting its impressive versatility for the fabrication of ultrathin 2D nanomaterials at room temperature. Especially, as illustrated by photographs in Fig. S5,† the production yield of ultrathin Ni_2Fe_1-LDHs nanosheets can easily reach up to gram level with increasing the volume of container, demonstrating the mass production of ultrathin NiFe-LDHs nanosheets, which is in favor of the future commercial utilization.

To investigate the electrocatalytic activity of different NiFe-LDHs samples for water oxidation, a series of electrochemical tests were performed in a three-electrode system on a glassy carbon (GC) electrode. First, cyclic voltammetry (CV) curves recorded at different potential sweep rates in 1 M KOH aqueous electrolyte are shown in Fig. S6,† from which evident oxidation peaks ascribe to the oxidation reaction of Ni^{2+} to Ni^{3+} can be well observed between 1.4 and 1.6 V *vs.* RHE. Obviously, upon the increase in sweep rate (ν) from 10 to 150 mV s^{-1}, the oxidation peaks demonstrate a corresponding increase in anodic current density (I_{pa}), which leads to a significant linear

correlation between the I_{pa} and $\nu^{1/2}$ as shown in Fig. 3A. The calculated slope value for Ni_2Fe_1-LDHs is greater than that for Ni_4Fe_1-LDHs, Ni_9Fe_1-LDHs and Ni_1Fe_1-LDHs, suggesting a better diffusion capacity of OH^- on the Ni_2Fe_1-LDHs sample in comparison with others, which is more favorable for the formation of electroactive high-valence species on catalyst surface to drive the water oxidation process.[27,28] Furthermore, the linear sweep voltammetry (LSV) curves (Fig. 3B) show that the anodic current density of NiFe-LDHs increases sharply with the increase of the applied potential over the oxidation peak, manifesting the conspicuous catalytic activity for the OER. Next, Fig. 3C reveals that the Ni_2Fe_1-LDHs sample gives a small overpotential (η) of 283 mV at a current density of 20 mA cm^{-2}, which is obviously lower than that of other NiFe-LDHs samples, signifying the less energy required to achieve a rapid OER rate. Notably, the Ni_2Fe_1-LDHs sample affords the highest water oxidation activity among these tested NiFe-LDHs samples, with a considerable anodic current density of up to 349.1 mA cm^{-2} at 1.8 V *vs.* RHE, much higher than that of reported IrO_2 and RuO_2 electrodes,[4,29] and even comparable to that of the best NiFe-based and perovskite-type electrocatalysts[30–32] under the similar condition (Table S4†). Moreover, the overpotential plotted against log(current density) in accordance with the Tafel equation was applied to study the catalytic kinetics for the OER. The corresponding Tafel plots in Fig. 3D show that the Tafel slope of Ni_2Fe_1-LDHs sample is calculated to be 60.0 mV per decade, marginally lower than that of Ni_4Fe_1-LDHs (88.5 mV per decade) and much smaller than that of Ni_9Fe_1-LDHs (126.5 mV per decade) and Ni_1Fe_1-LDHs (135.5 mV per decade), which is of indicative the largely accelerated OER rate with a facile increase in applied voltage by using the Ni_2Fe_1-LDHs electrode. Moreover, the electrochemical impedance spectroscopy (EIS) is carried out to gain insights into the electrode kinetics toward OER. Clearly, the Nyquist plots in Fig. 4A uncover that the charge-transfer resistance of Ni_2Fe_1-LDHs sample demonstrates a noticeable decrease in comparison to other NiFe-LDHs samples, undoubtedly confirming its more favourable charge transfer kinetics for the OER. In addition, the electrocatalytic OER activities of obtained CoFe- and NiCo-based ultrathin nanosheets were also measured and the collected LSV curves are present in Fig. S7.† As can be seen, some of the tested samples show impressive OER activity, with low overpotentials, large anodic current densities and small Tafel slopes. In comparison, Ni_2Fe_1-LDHs gives the highest OER activity among these catalysts, distinctly embodying its superiority in electrochemical water oxidation.

As well accepted, the electrochemical active surface area (ECSA) has been regarded as a key parameter for determining the electrocatalytic activity, which is positively associated with the double layer capacitance (C_{dl}).[33,34] As shown in Fig. S8,† the C_{dl} was tested by CV curves at diverse scan rates ranging from 1 to 10 mV s^{-1} in a non-faradaic potential region. Fig. 4B displays that the C_{dl} values of Ni_2Fe_1-LDHs and Ni_4Fe_1-LDHs are respectively estimated to be 950.4 μF cm^{-2} and 729.7 μF cm^{-2}, larger than that of Ni_1Fe_1-LDHs (542.8 μF cm^{-2}) and Ni_9Fe_1-LDHs (703.1 μF cm^{-2}), which indeed demonstrates the higher electrochemical active surface areas of Ni_1Fe_1-LDHs and Ni_4Fe_1-LDHs related to the more exposed active sites. Especially, the LSV curves were normalized by the corresponding C_{dl} values to gain more insights into the electrocatalytic OER activity. As can be seen from Fig. 4C, the normalized anodic current density of

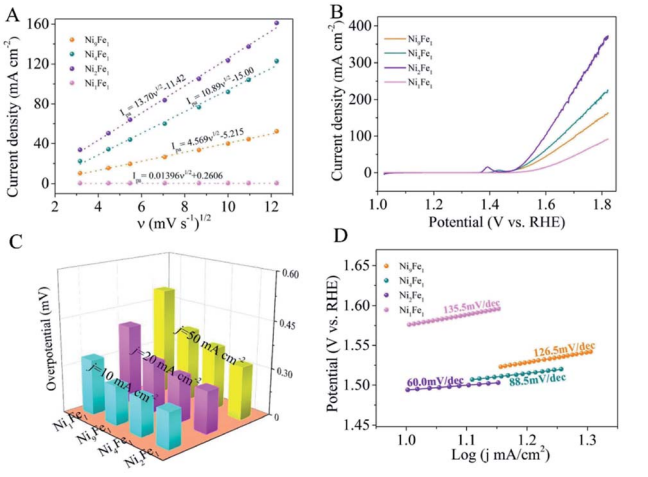

Fig. 3 Electrochemical tests for the OER performance of various NiFe-LDHs samples in 1 M KOH solution. (A) Linear correlation between the I_{pa} and the $\nu^{1/2}$. (B) Polarization curves and (C) the overpotentials required for different current densities and (D) corresponding Tafel plots.

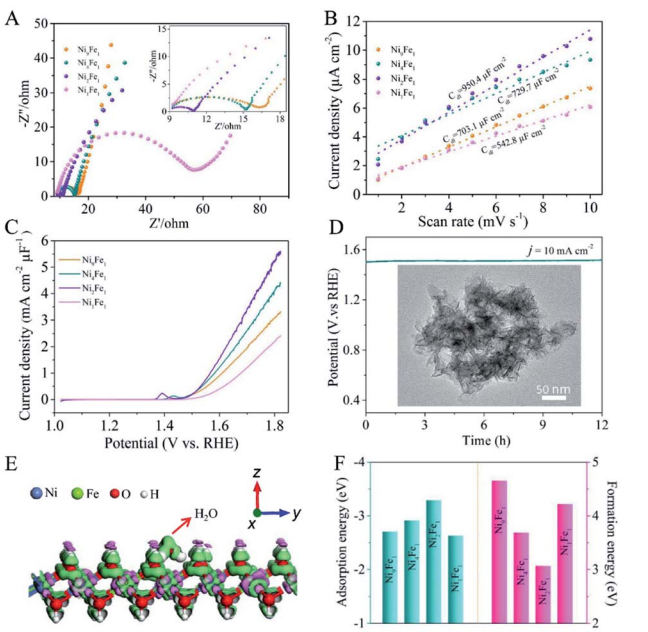

Fig. 4 (A) Nyquist impedance plots, (B) current density plotted *versus* scan rate for the estimation of C_{dl} values and (C) the normalized LSV curves of various NiFe-LDHs samples. (D) Chronopotentiometric measurement of Ni_2Fe_1-LDHs sample at a constant current density of 10 mA cm^{-2} for 12 h. The inset in (D) shows the TEM image of Ni_2Fe_1-LDHs sample after the long-term stability test. (E) Illustration of the adsorption of water molecule on the Ni_2Fe_1-LDHs and the corresponding differential charge density. (F) The calculated formation energies of electroactive NiOOH species and adsorption energies of water molecules onto the surface of different NiFe-LDHs samples.

Ni_2Fe_1-LDHs (5.6 mA cm^{-2}) is roughly 1.3, 1.7 and 2.3 times larger than that of Ni_4Fe_1-LDHs (4.4 mA cm^{-2}), Ni_9Fe_1-LDHs (3.3 mA cm^{-2}) and Ni_1Fe_1-LDHs (2.4 mA cm^{-2}) at the overpotential of 592 mV, respectively, indicating the superior intrinsic catalytic activity of every reactive center in the Ni_2Fe_1-LDHs sample. Apart from the catalytic activity, long-term stability is another vital criterion for the assessment of advanced electrocatalysts for the OER. Fig. 4D shows the chronopotentiometric test at an invariable current density ($J = 10$ mA cm^{-2}) for Ni_2Fe_1-LDHs, from which negligible changes in potential can be identified even after continuous 12 h operation in 1 M KOH solution, revealing its excellent catalytic stability. Besides, TEM image (inset of Fig. 4D) demonstrates slight variations in morphology of Ni_2Fe_1-LDHs sample after the long-term stability measurement, verifying its impressive structural durability. On the basis of above results, the Ni_2Fe_1-LDHs sample gives prominent electrocatalytic OER activity and robust stability, which is in favour of potential practical applications for electrocatalytic water splitting.

To get insights into the impact of Ni/Fe atomic ratios on the electronic structures of NiFe-LDHs samples, density functional theory (DFT) calculations were carried out by using NiFe-LDHs with different Ni/Fe ratios as applicable models. As well accepted, water molecules should be proactively adsorbed on the surface of catalysts, which means that the adsorption of H_2O molecules plays a decisive role in determining the OER performance.[8,35] From the differential charge density in Fig. 4E, a notable charge transfer between water molecule and Ni_4Fe_1-LDHs can be well observed, reflecting its famous electrocatalytic reactivity toward water oxidation. Furthermore, as shown in Fig. 4F and Table S2,† the adsorption energies of H_2O molecules on the NiFe-LDHs surface are calculated to be about −2.71, −2.92, −3.29 and −2.63 eV for Ni_9Fe_1-, Ni_4Fe_1-, Ni_2Fe_1- and Ni_1Fe_1-LDHs sample, respectively. The smallest adsorption energy for Ni_2Fe_1-LDHs means that the water molecule is more easily adsorbed onto the surface of Ni_2Fe_1-LDHs with respect to the other three samples, thus achieving optimized OER kinetics to promote the catalytic process. Besides, for the NiFe-LDHs catalyst, the formation energy of NiOOH species is another important factor that influences the whole OER activity of catalyst, as the high-valence NiOOH phase has been deemed as electroactive species for the OER.[31,36–38] As displayed in Fig. 4F and Table S3,† the calculated formation energy of active NiOOH species for Ni_2Fe_1-LDHs sample is about 3.07 eV, obviously lower than that for Ni_9Fe_1-LDHs (4.66 eV), Ni_4Fe_1-LDHs (3.69 eV) and Ni_1Fe_1-LDHs (4.22 eV). This result demonstrates that the Ni_2Fe_1-LDHs sample is more favourable for the formation of electroactive NiOOH phase, thereby obtaining accelerated electrochemical OER process. Based on the experimental and theoretical data, the Ni_2Fe_1-LDHs sample gives prominent electrocatalytic OER activity and robust stability, which is mainly attributed to two aspects as follows: (1) the ultrathin 2D structure not only renders highly exposed metal atoms as active sites to promote the catalytic reaction, but also enables a better contact with the GC electrode and electrolyte as well as good electrical conductivity to accelerate electron transfer. (2) The tunable component with an optimal Ni/Fe ratio is beneficial to the synergetic optimization of the adsorption energy of H_2O molecules and formation energy of active NiOOH species as well as the charge transfer during the electrocatalytic process, thus realizing highly efficient OER.

Conclusions

In summary, ultrathin NiFe-LDHs nanosheets with adjustable components and mass production yield were synthesized at room temperature through a simple and fast co-precipitation route, which were further taken as examples to investigate the effect of Ni/Fe ratio on the OER activity through combining theoretical calculations and experimental measurements. Benefiting from plenty of catalytically active sites, efficient electron transport and optimal OER kinetics, the as-prepared ultrathin NiFe-LDHs nanosheets were proved as highly active electrocatalysts for water oxidation application. It was found that Ni_2Fe_1-LDHs exhibits a small overpotential of 263 mV to reach 10 mA cm^{-2} and large current density of 349.1 mA cm^{-2} at a potential of 1.8 V *vs.* RHE, as well as excellent long-term OER stability in strong alkaline solution. This work opens up a pathway for large-scale synthesis of efficient transition-metal-based LDHs catalysts for water oxidation at low cost.

Conflicts of interest

There are no conflicts to declare.

Acknowledgements

This work was supported by the National Natural Science Foundation of China (21805149, 21675093), the Natural Science Foundation of Shandong Province of China (ZR2018BB012, 2015ZRB01A0D), the Taishan Scholar Program of Shandong Province of China (ts20110829).

Notes and references

1 S. Y. Reece, J. A. Hamel, K. Sung, T. D. Jarvi, A. J. Esswein, J. J. H. Pijpers and D. G. Nocera, Wireless solar water splitting using silicon-based semiconductors and earth-abundant catalysts, *Science*, 2011, **334**, 645–648.

2 J. Suntivich, K. J. May, H. A. Gasteiger, J. B. Goodenough and S. H. Yang, A perovskite oxide optimized for oxygen evolution catalysis from molecular orbital principles, *Science*, 2011, **334**, 1383–1385.

3 Q. He, Y. Y. Wan, H. L. Jiang, Z. W. Pan, C. Q. Wu, M. Wang, X. J. Wu, B. J. Ye, P. M. Ajayan and L. Song, *ACS Energy Lett.*, 2018, **3**, 1373–1380.

4 J. Q. Yan, L. Q. Kong, Y. J. Ji, J. White, Y. Y. Li, J. Zhang, P. F. An, S. Z. Liu, S. T. Lee and T. Y. Ma, Nickel vacancies boost reconstruction in nickel hydroxide electrocatalyst, *Nat. Commun.*, 2019, **10**, 2149.

5 D. Li, H. Baydoun, C. N. Verani and S. L. Brock, Efficient water oxidation using CoMnP nanoparticles, *J. Am. Chem. Soc.*, 2016, **138**, 4006–4009.

6 S. W. Lee, C. Carlton, M. Risch, Y. Surendranath, S. Chen, S. Furutsuki, A. Yamada, D. G. Nocera and S. H. Yang, The nature of lithium battery materials under oxygen evolution

reaction conditions, *J. Am. Chem. Soc.*, 2012, **134**, 16959–16962.

7 M. Gong, Y. G. Li, H. L. Wang, Y. Y. Liang, J. Z. Wu, J. G. Zhou, J. Wang, T. Regier, F. Wei and H. J. Dai, An advanced Ni–Fe layered double hydroxide electrocatalyst for water oxidation, *J. Am. Chem. Soc.*, 2013, **135**, 8452–8455.

8 J. Bao, X. D. Zhang, B. Fan, J. J. Zhang, M. Zhou, W. L. Yang, X. Hu, H. Wang, B. C. Pan and Y. Xie, Ultrathin spinel-structured nanosheets rich in oxygen deficiencies for enhanced electrocatalytic water oxidation, *Angew. Chem., Int. Ed.*, 2015, **54**, 7399–7404.

9 J. B. Gerken, J. G. McAlpin, J. Y. C. Chen, M. L. Rigsby, W. H. Casey, R. D. Britt and S. S. Stahl, Electrochemical water oxidation with cobalt-based electrocatalysts from pH 0–14: the thermodynamic basis for catalyst structure, stability, and activity, *J. Am. Chem. Soc.*, 2011, **133**, 14431–14442.

10 F. A. Frame, T. K. Townsend, R. L. Chamousis, E. M. Sabio, T. Dittrich, N. D. Browning and F. E. Osterloh, Photocatalytic water oxidation with nonsensitized IrO_2 nanocrystals under visible and UV light, *J. Am. Chem. Soc.*, 2011, **133**, 7264–7267.

11 F. Song and X. L. Hu, Ultrathin cobalt–manganese layered double hydroxide is an efficient oxygen evolution catalyst, *J. Am. Chem. Soc.*, 2014, **136**, 16481–16484.

12 L. Trotochaud, S. L. Young, J. K. Ranney and S. W. Boettcher, Nickel–Iron oxyhydroxide oxygen-evolution electrocatalysts: the role of intentional and incidental iron incorporation, *J. Am. Chem. Soc.*, 2014, **136**, 6744–6753.

13 F. Dionigi, Z. H. Zeng, L. Sinev, T. Merzdorf, S. Deshpande, M. B. Lopez, S. Kunze, I. Zegkinoglou, H. Sarodnik, D. X. Fan, A. Bergmann, J. Drnec, J. F. Araujo, M. Gliech, D. Teschner, J. Zhu, W. X. Li, J. Greeley, B. R. Cuenya and P. Strasser, In situ structure and catalytic mechanism of NiFe and CoFe layered double hydroxides during oxygen evolution, *Nat. Commun.*, 2020, **11**, 2522.

14 D. W. Wang, Q. Li, C. Han, Q. Q. Lu, Z. C. Xing and X. R. Yang, Atomic and electronic modulation of self-supported nickel-vanadium layered double hydroxide to accelerate water splitting kinetics, *Nat. Commun.*, 2019, **10**, 3899.

15 R. Chen, S. F. Hung, D. J. Zhou, J. J. Gao, C. J. Yang, H. B. Tao, H. B. Yang, L. P. Zhang, L. L. Zhang, Q. H. Xiong, H. M. Chen and B. Liu, Layered Structure causes bulk NiFe layered double hydroxide unstable in alkaline oxygen evolution reaction, *Adv. Mater.*, 2019, **31**, 1903909.

16 M. P. Browne, Z. Sofer and M. Pumera, Layered and two dimensional metal oxides for electrochemical energy conversion, *Energy Environ. Sci.*, 2019, **12**, 41–58.

17 G. L. Fan, F. Li, D. G. Evans and X. Duan, Catalytic applications of layered double hydroxides: recent advances and perspectives, *Chem. Soc. Rev.*, 2014, **43**, 7040–7066.

18 L. N. Dang, H. F. Liang, J. Q. Zhuo, B. K. Lamb, H. Y. Sheng, Y. Yang and S. Jin, Direct synthesis and anion exchange of noncarbonate-intercalated NiFe-layered double hydroxides and the influence on electrocatalysis, *Chem. Mater.*, 2018, **30**, 4321–4330.

19 Y. F. Sun, S. Gao, F. C. Lei, C. Xiao and Y. Xie, Ultrathin two-dimensional inorganic materials: new opportunities for solid state nanochemistry, *Acc. Chem. Res.*, 2015, **48**, 3–12.

20 W. L. Yang, X. D. Zhang and Y. Xie, Advances and challenges in chemistry of two-dimensional nanosheets, *Nano Today*, 2016, **11**, 793–816.

21 Q. Wang and D. O'Hare, Recent advances in the synthesis and application of layered double hydroxide (LDH) nanosheets, *Chem. Rev.*, 2012, **112**(7), 4124–4155.

22 J. F. Yu, Q. Wang, D. O'Hare and L. Y. Sun, Preparation of two dimensional layered double hydroxide nanosheets and their applications, *Chem. Soc. Rev.*, 2017, **46**, 5950–5974.

23 H. C. Yang, C. H. Wang, Y. J. Zhang and Q. B. Wang, Green synthesis of NiFe LDH/Ni foam at room temperature for highly efficient electrocatalytic oxygen evolution reaction, *Sci. China Mater.*, 2019, **62**, 681–689.

24 M. A. Oliver-Tolentino, J. Vazquez-Samperio, A. Manzo-Robledo, R. D. G. Gonzalez-Huerta, J. L. Flores-Moreno, D. Ramírez-Rosales and A. Guzman-Vargas, An approach to understanding the electrocatalytic activity enhancement by superexchange interaction toward OER in alkaline media of Ni–Fe LDH, *J. Phys. Chem. C*, 2014, **118**, 22432–22438.

25 J. H. Zhao, L. L. Cai, H. Li, X. J. Shi and X. L. Zheng, Stabilizing silicon photocathodes by solution-deposited Ni–Fe layered double hydroxide for efficient hydrogen evolution in alkaline media, *ACS Energy Lett.*, 2017, **2**, 1939–1946.

26 J. D. Chen, F. Zheng, S. J. Zhang, A. Fisher, Y. Zhou, Z. Y. Wang, Y. Y. Li, B. B. Xu, J. T. Li and S. G. Sun, Interfacial interaction between FeOOH and Ni–Fe LDH to modulate the local electronic structure for enhanced OER electrocatalysis, *ACS Catal.*, 2018, **8**, 11342–11351.

27 S. Xie, X. L. Tong, G. Q. Jin, Y. Qin and X. Y. Guo, CNT–Ni/SiC hierarchical nanostructures: preparation and their application in electrocatalytic oxidation of methanol, *J. Mater. Chem. A*, 2013, **1**, 2104–2109.

28 C. M. Hou, W. L. Yang, X. P. Yang, B. J. Li, H. T. Gao and X. L. Luo, In situ sulfidation for controllable hetero-interface engineering of α-$Ni(OH)_2$–Ni_3S_4 hybrid structures realizing robust electrocatalytic methanol oxidation, *Chem. Commun.*, 2020, **56**, 5283–5286.

29 J. H. Huang, J. T. Chen, T. Yao, J. F. He, S. Jiang, Z. H. Sun, Q. H. Liu, W. Cheng, F. C. Hu, Y. Jiang, Z. Y. Pan and S. Q. Wei, CoOOH nanosheets with high mass activity for water oxidation, *Angew. Chem., Int. Ed.*, 2015, **54**, 8722–8727.

30 F. Song and X. L. Hu, Exfoliation of layered double hydroxides for enhanced oxygen evolution catalysis, *Nat. Commun.*, 2014, **5**, 4477.

31 J. F. Xie, J. P. Xin, R. X. Wang, X. D. Zhang and F. C. Lei, Sub-3 nm pores in two-dimensional nanomesh promoting the generation of electroactive phase for robust water oxidation, *Nano Energy*, 2018, **53**, 74–82.

32 H. P. Wang, J. Wang, Y. C. Pi, Q. Shao, Y. M. Tan and X. Q. Huang, Double perovskite $LaFexNi_{1-x}O_3$ nanorods enable efficient oxygen evolution electrocatalysis, *Angew. Chem., Int. Ed.*, 2019, **58**, 2316–2320.

33 J. Kibsgaard, Z. Chen, B. N. Reinecke and T. F. Jaramillo, Engineering the surface structure of MoS_2 to preferentially expose active edge sites for electrocatalysis, *Nat. Mater.*, 2012, **11**, 963–969.

34 D. Merki, H. Vrubel, L. Rovelli, S. Fierro and X. L. Hu, Fe, Co, and Ni ions promote the catalytic activity of amorphous molybdenum sulfide films for hydrogen evolution, *Chem. Sci.*, 2012, **3**, 2515–2525.

35 Y. F. Sun, S. Gao, F. C. Lei, J. W. Liu, L. Liang and Y. Xie, Atomically-thin non-layered cobalt oxide porous sheets for highly efficient oxygen-evolving electrocatalysts, *Chem. Sci.*, 2014, **5**, 3976–3982.

36 Q. He, Y. Y. Wan, H. L. Jiang, Z. W. Pan, C. Q. Wu, M. Wang, X. J. Wu, B. J. Ye, P. M. Ajayan and L. Song, Nickel vacancies boost reconstruction in nickel hydroxide electrocatalyst, *ACS Energy Lett.*, 2018, **3**, 1373–1380.

37 L. Trotochaud, J. K. Ranney, K. N. Williams and S. W. Boettcher, Nickel−Iron Oxyhydroxide Oxygen-Evolution Electrocatalysts: The Role of Intentional and Incidental Iron Incorporation, *J. Am. Chem. Soc.*, 2012, **134**, 17253–17261.

38 M. R. Gao, W. G. Sheng, Z. B. Zhuang, Q. R. Fang, S. Gu, J. Jiang and Y. S. Yan, Efficient Water Oxidation Using Nanostructured α-Nickel-Hydroxide as an Electrocatalyst, *J. Am. Chem. Soc.*, 2014, **136**, 7077–7084.

39 G. Kresse and J. Furthmuller, Efficient iterative schemes for ab initio total-energy calculations using a plane-wave basis set, *Phys. Rev. B: Condens. Matter Mater. Phys.*, 1996, **54**, 11169.

40 J. Hafner, Ab Initio Simulations of Materials Using VASP: Density-Functional Theory and Beyond, *J. Comput. Chem.*, 2008, **29**, 2044.

41 J. P. Perdew, A. Ruzsinszky, G. I. Csonka, O. A. Vydrov, G. E. Scuseria, L. A. Constantin, X. Zhou and K. Burke, Restoring the Density-Gradient Expansion for Exchange in Solids and Surfaces, *Phys. Rev. Lett.*, 2008, **101**, 136406.

42 A. I. Liechtenstein, V. I. Anisimov and J. Zaanen, Density-functional theory and strong interactions: orbital ordering in Mott-Hubbard insulators, *Phys. Rev. B: Condens. Matter Mater. Phys.*, 1995, **52**, R5467.

43 S. Grimme, J. Antony, S. Ehrlich and H. Krieg, A consistent and accurate ab initio parametrization of density functional dispersion correction (DFT-D) for the 94 elements H-Pu, *J. Chem. Phys.*, 2010, **132**, 154104.